INTERNATIONAL JOURNAL FOR NUMERICAL METHODS IN ENGINEERING
Int. J. Numer. Meth. Engng 2013; **00**:1–21
Published online in Wiley InterScience (www.interscience.wiley.com). DOI: 10.1002/nme

An isogeometric analysis Bézier interface element for mechanical and poromechanical fracture problems

Faisal Irzal[1], Joris J. C. Remmers[1], Clemens V. Verhoosel[1], René de Borst[2*]

[1]*Eindhoven University of Technology, Department of Mechanical Engineering, PO BOX 513, 5600 MB, Eindhoven, The Netherlands.*
[2]*University of Glasgow, School of Engineering, Rankine Building, Oakfield Avenue, Glasgow G12 8LT, UK.*

SUMMARY

Interface elements are a powerful tool for modelling discontinuities. Herein, we develop an interface element that is based on the isogeometric analysis concept. Through Bézier extraction the novel interface element can be cast in the same format as conventional interface elements. Consequently, the isogeometric interface element can be implemented in a straightforward manner in existing finite element software by a mere redefinition of the shape functions. The interface elements share the advantages of isogeometric continuum elements in that they can exactly model the geometry. On the other hand, they inherit the simplicity of conventional interface elements, but also some deficiencies, like the occurrence of traction oscillations when a high interface stiffness is used. The extension towards poroelasticity is rather straightforward, and in this situation the smoother flow profiles and the ensuing preservation of local mass balance are additional advantages. These are demonstrated at the hand of some example problems.

Received . . .

KEY WORDS: Cohesive zone model, crack propagation, isogeometric analysis; B-splines; Bézier extraction

1. INTRODUCTION

Zero-thickness interface elements have been an important tool for modelling discontinuities such as cracks, faults and shear bands since the early 1990s, e.g., [1, 2, 3]. Their availability in many commercial software packages and their easy use have made them popular for a range of applications, including fracture in ductile and quasi-brittle materials, delamination in composites, and shear band formation in sand and other granular materials. More recently, they have been extended to include fluid flow in fully saturated granular materials in Reference [4].

Interface elements are easy to use, but their applicability is restricted to stationary discontinuities, or to situations where the path along which the discontinuity will evolve is known a priori [1], as in lamellar materials [5, 6, 7]. A first step towards the arbitrary propagation of discontinuities, in which the path along which the discontinuity can evolve is not known in advance, was made by Xu and Needleman [8], who inserted interface elements between *all* continuum elements. A more rigorous approach is to apply remeshing at each load or time increment, as in [9, 10]. The extension of remeshing schemes to poroelasticity was made in Reference [11] for the simulation of hydraulically

*Correspondence to: René de Borst, University of Glasgow, School of Engineering, Oakfield Avenue, Rankine Building, Glasgow G12 8LT, UK. E-mail: Rene.DeBorst@glasgow.ac.uk
†Please ensure that you use the most up to date class file, available from the NME Home Page at
http://www3.interscience.wiley.com/journal/1430/home

driven fracture propagation using linear elastic fracture mechanics, and in Reference [12] for modelling hydraulic cohesive crack growth.

Exploiting the partition of unity property of finite element shape functions, an elegant method to allow for arbitrary crack propagation without remeshing was introduced by Belytschko and co-workers [13, 14] for linear elastic fracture mechanics, while the extension towards cohesive fracture was made in [15, 16, 17, 18]. In a series of papers de Borst and co-workers showed how this concept can be extended to crack and shear band propagation in fluid-saturated media [19, 20, 21, 22, 23].

Exploiting the possibility to simply lower the order of spline functions, Verhoosel *et al.* [24], introduced arbitrary discontinuities in isogeometric analysis. The present paper builds upon this development, and simplifies it in the sense that an isogeometric equivalent of interface elements is developed, which is easy to implement in standard finite element software. This holds in particular since it has been formulated using Bézier extraction, which makes it compatible with standard finite element datastructures, see Borden *et al.* [25] for continua modelled using NURBS, and Scott *et al.* [26] for the extension to T-splines. As indicated in the preceding, fracture in geotechnical engineering, petroleum engineering and in biomechanical engineering usually involves fluid-saturated porous media. For this reason, we have extended the Bézier interface element to situations where fluid flow in the interface and in the surrounding poroelastic medium become important.

To provide a proper setting, we begin with a brief summary of the relevant physics in Section 2. In Section 3 we review some fundamental concepts of isogeometric analysis and the concept of Bézier extraction, which enables to cast isogeometric analysis in a standard finite element format. The weak form and the discretisation scheme are presented in Section 4. It is shown that the Bézier interface element inherits many properties of standard interface elements, but salient differences are also pointed out. Numerical examples on mechanical and poromechanical problems demonstrate the possibilities of the approach in Section 5.

2. GOVERNING EQUATIONS

In this section, we briefly summarize the problem of interest and the governing equations. The section is divided in two parts; one related to the description of the mechanical problem, while the next part describes the poromechanical problem. In the first part, the discontinuity is introduced as an internal boundary equipped with a traction-separation relation. In the second part, the behaviour of the bulk material is modelled using an elementary poroelasticity theory, while the traction-separation relation over the interface is supplemented by a local mass balance equation to take into account the fluid flow in the discontinuity.

2.1. Mechanical problem

We consider a body $\boldsymbol{\Omega}$ which is crossed by a discontinuity Γ_{d}. The displacement of the material point $\mathbf{x} \in \boldsymbol{\Omega}$ is described by the displacement vector field $\mathbf{u}$. The external boundary of the body is composed of a boundary Γ_u, on which essential boundary conditions are provided, and a boundary Γ_t with natural boundary conditions. The internal boundary Γ_{d} represents an adhesive interface between two parts of the domain.

Under the assumption of small displacements and small displacement gradients, the deformation of the solid matrix is described by the infinitesimal strain tensor $\boldsymbol{\varepsilon} = \frac{1}{2}\left(\nabla\mathbf{u} + (\nabla\mathbf{u})^{\mathrm{T}}\right)$. The crack opening $\mathbf{v}$ is defined as the difference between the displacement on either side of the internal boundary Γ_{d}. In the absence of body forces, the strong form of the quasi-static equilibrium equations for the solid material are given by:

$$\begin{cases} \nabla \cdot \boldsymbol{\sigma} = \mathbf{0} & \mathbf{x} \in \boldsymbol{\Omega} \\ \mathbf{u} = \bar{\mathbf{u}} & \mathbf{x} \in \boldsymbol{\Gamma}_u \\ \mathbf{n} \cdot \boldsymbol{\sigma} = \bar{\mathbf{t}} & \mathbf{x} \in \boldsymbol{\Gamma}_t \\ \mathbf{n}_{\Gamma_{\mathrm{d}}} \cdot \boldsymbol{\sigma} = \mathbf{t}(\mathbf{v}) & \mathbf{x} \in \boldsymbol{\Gamma}_{\mathrm{d}} \end{cases} \tag{1}$$

DOI: 10.1002/nme

with $\boldsymbol{\sigma}$ the Cauchy stress tensor and $\mathbf{n}$ is the vector normal to a boundary. The prescribed displacement and traction at the boundary are given by $\bar{\mathbf{u}}$ and $\bar{\mathbf{t}}$, respectively.

We assume that the stress rate in the bulk material, $\dot{\boldsymbol{\sigma}}$, is linearly related to the strain rate $\dot{\boldsymbol{\varepsilon}}$ through a linear stress-strain relation:

$$\dot{\boldsymbol{\sigma}} = \mathbf{D} : \dot{\boldsymbol{\varepsilon}} \tag{2}$$

where $\mathbf{D}$ represents the fourth-order tangential stiffness tensor of the bulk material. In the examples, a linear elastic, rate-independent constitutive relation has been used. The traction at the discontinuity $\boldsymbol{\Gamma}_\mathrm{d}$ is expressed in terms of the corresponding local displacement jumps $\mathbf{v}_\mathrm{d}$:

$$\dot{\mathbf{t}}_\mathrm{d} = \mathbf{T}_\mathrm{d} \cdot \dot{\mathbf{v}}_\mathrm{d} \tag{3}$$

where $\mathbf{t}_\mathrm{d}$ denotes the tractions defined in a local coordinate system which is aligned with the discontinuity and $\mathbf{T}_\mathrm{d}$ is the tangent stiffness of the traction-separation relation.

Restricting the treatment to a two-dimensional configuration, the tractions can be written as: $\mathbf{t}_\mathrm{d} = t_n \mathbf{n}_{\Gamma_\mathrm{d}} + t_s \mathbf{t}_{\Gamma_\mathrm{d}}$, where t_n and t_s are the normal traction and the shear traction. The local displacement jump $\mathbf{v}_\mathrm{d}$ is denoted by $\mathbf{v}_\mathrm{d} = v_n \mathbf{n}_{\Gamma_\mathrm{d}} + v_s \mathbf{t}_{\Gamma_\mathrm{d}}$, so that the transformation of the constitutive relation (3) to the global coordinate system results in:

$$\dot{\mathbf{t}} = \mathbf{R}^\mathrm{T} \cdot \dot{\mathbf{t}}_\mathrm{d} = \mathbf{R}^\mathrm{T} \cdot \mathbf{T}_\mathrm{d} \cdot \dot{\mathbf{v}}_\mathrm{d} = \mathbf{R}^\mathrm{T} \cdot \mathbf{T}_\mathrm{d} \cdot \mathbf{R}\dot{\mathbf{v}} = \mathbf{T} \cdot \dot{\mathbf{v}} \tag{4}$$

with $\mathbf{R}$ the standard rotation tensor, e.g. [27].

2.2. *Poromechanical problem*

Next, an isotropic fully saturated porous medium is considered, which consists of a solid matrix and an interstitial fluid. The balance of momentum, Equation (1), is now supplemented by the mass balance:

$$\begin{cases} \alpha \nabla \cdot \dot{\mathbf{u}} + M^{-1} \dot{p}_\mathrm{f} + \nabla \cdot \mathbf{q} = 0 & \mathbf{x} \in \Omega \\ p_\mathrm{f} = \bar{p} & \mathbf{x} \in \Gamma_p \\ \mathbf{n} \cdot \mathbf{q} = \bar{q} & \mathbf{x} \in \Gamma_q \\ \mathbf{n}_{\Gamma_\mathrm{d}} \cdot \mathbf{q} = q_\mathrm{d} & \mathbf{x} \in \Gamma_\mathrm{d} \end{cases} \tag{5}$$

with $\boldsymbol{\sigma}$ the total stress tensor defined as:

$$\boldsymbol{\sigma} = \boldsymbol{\sigma}_\mathrm{eff} - \alpha p_\mathrm{f} \mathbf{I} \tag{6}$$

and $\boldsymbol{\sigma}_\mathrm{eff}$ is the effective stress of the solid skeleton, α is the Biot-Willis coefficient, p_f is the pore fluid pressure and $\mathbf{I}$ is the second-order unit tensor. Herein,

$$M^{-1} = (\alpha - \phi)/K_\mathrm{s} + \phi/K_\mathrm{f}$$

is the constrained specific storage of the porous medium, i.e. the inverse of the Biot coefficient M, that is governed by the porosity of the medium ϕ and by the compressibility of the solid and fluid constituents, denoted by K_s and K_f, respectively. The flow of the pore fluid is assumed to obey Darcy's relation:

$$\mathbf{q} = -\frac{k}{\mu} \nabla p_\mathrm{f} \tag{7}$$

with k the intrinsic permeability of the porous medium and μ is the dynamic viscosity of the interstitial fluid.

As in purely mechanical problems, the traction at the discontinuity $\mathbf{t}_\mathrm{d} = \mathbf{t}_\mathrm{d}(\mathbf{v}_\mathrm{d})$ is captured using a traction-separation, or cohesive-surface relation as in Equation (3). However, the traction from the solid at the interface is now coupled to the pressure of the fluid. Assuming stress continuity from the cavity to the bulk, we have:

$$\mathbf{n}_{\Gamma_\mathrm{d}} \cdot \boldsymbol{\sigma} = \mathbf{t}_\mathrm{d} - p_\mathrm{f} \mathbf{n}_{\Gamma_\mathrm{d}} \tag{8}$$

When the mass balance, Equation (5), is interpreted as a global mass balance equation for the entire body, and is cast into a weak format, a surface integral at the internal discontinuity Γ_d arises

Prepared using nmeauth.cls
DOI: 10.1002/nme

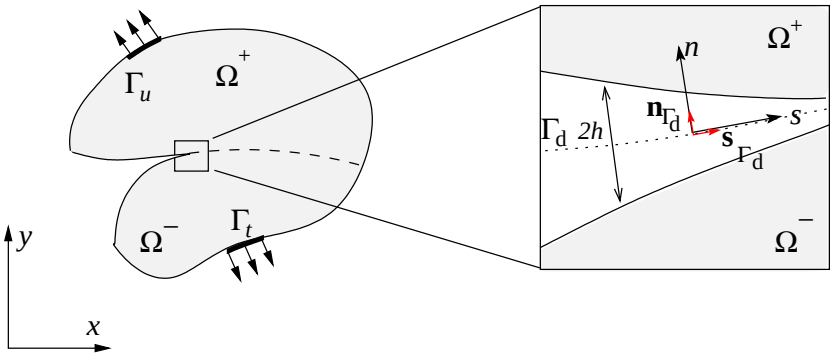

Figure 1. Local and global coordinate systems in the discontinuity.

with the integrand $\mathbf{n}_{\Gamma_\mathrm{d}} \cdot \mathbf{q}$. This term can be quantified by averaging the *local* mass balance, which is also given by Equation (5), over the opening of the discontinuity [19, 20, 21, 22, 23]:

$$\int_{-h}^{h} \left(\alpha \nabla \cdot \dot{\mathbf{u}} + \frac{1}{M} \dot{p}_\mathrm{f} + \nabla \cdot \mathbf{q} \right) \mathrm{d}n = 0. \tag{9}$$

In this equation, $2h$ is the normal opening of the discontinuity, see Figure 1. Defining the local (s, n) coordinate system and taking into account that the crack opening is small compared to its length, the integral can be approximated to give:

$$\mathbf{n}_{\Gamma_\mathrm{d}} \cdot \mathbf{q} = 2h \frac{\partial q_s}{\partial s} - \frac{2h}{M} \dot{p}_\mathrm{f} - 2h\alpha \langle \frac{\partial \dot{u}_s}{\partial s} \rangle - 2\alpha \dot{h}. \tag{10}$$

with q_s the relative fluid velocity in the tangential direction:

$$q_s = -\frac{h^2}{12\mu} \frac{\partial p_\mathrm{f}}{\partial s} \tag{11}$$

and $\langle \frac{\partial \dot{u}_s}{\partial s} \rangle$ represents the average value of the tangential acceleration of the solid phase at the discontinuity faces. Upon substitution of Equation (11) into (10) it can be observed that the interfacial flux $\mathbf{n}_{\Gamma_\mathrm{d}} \cdot \mathbf{q}$ is proportional to the second spatial derivative of the pore fluid pressure p_f.

3. ISOGEOMETRIC FINITE ELEMENT ANALYSIS

An advantage of isogeometric analysis over traditional finite element analysis is the possibility to control inter-element continuity conditions. This evidently facilitates the discretisation of higher-order differential equations as encountered in e.g. phase field models [28] or gradient-damage models [29]. Besides the possibility to increase the inter-element order of continuity, isogeometric analysis also offers the possibility to (locally) reduce this continuity. In [24] it was demonstrated how this concept can be used to model discrete cracks. Here, we briefly review this isogeometric analysis approach for creating discontinuities, and then we propose a Bézier interface element as a finite element data structure that can be incorporated in standard finite element programs.

3.1. Discontinuities in B-splines

The key idea of isogeometric analysis is to use the basis functions used for the parametrisation of the geometry in computer-aided design (CAD) also for discretisation purposes. The introduction of discontinuities in isogeometric analysis is here discussed for B-splines. B-splines are the fundamental technology underlying Non-Uniform Rational B-splines (NURBS), which is the

DOI: 10.1002/nme

industry standard technology in CAD, and many state-of-the-art technologies such as e.g. T-splines. We refer to [30] for a detailed discussion of introducing discontinuities in NURBS and T-splines.

A univariate B-spline is a piecewise polynomial defined over a (non-decreasing) knot vector $\Xi = \{\xi_1, \xi_2, \cdots, \xi_{n+p+1}\}$, with n and p denoting the number and order[†] of basis functions, respectively [31]. For analysis purposes open B-splines are generally used, which are constructed by taking the multiplicity of the first and last knot value equal to $p+1$. The knot vector Ξ partitions the parameter domain, $\widehat{\Omega} = [\xi_1, \xi_{n+p+1}]$, into m segments of positive length, which are referred to as elements. B-spline basis functions over this parameter domain of order p, $\{N_{i,p}\}_{i=1}^{n}$, are defined recursively, starting with the zeroth-order $(p = 0)$ functions

$$N_{i,0}(\xi) = \begin{cases} 1 & \xi_i \leq \xi < \xi_{i+1} \\ 0 & \text{otherwise} \end{cases} \tag{12}$$

after which the higher-order basis functions ($p > 0$) are defined using the Cox-De Boor recursion relation [32, 33]

$$N_{i,p}(\xi) = \frac{\xi - \xi_i}{\xi_{i+p} - \xi_i} N_{i,p-1}(\xi) + \frac{\xi_{i+p+1} - \xi}{\xi_{i+p+1} - \xi_{i+1}} N_{i+1,p-1}(\xi). \tag{13}$$

In the context of modelling discontinuities, the primary property of interest of B-spline basis functions is their inter-element continuity. B-spline basis functions are $\mathcal{C}^{p-1}$ continuous over the element boundaries corresponding to non-repeated internal knots, which is in contrast to standard Lagrange finite element bases which are only $\mathcal{C}^0$ continuous over the element boundaries (regardless of their polynomial order). The number of continuous derivatives over a particular element boundary is decreased by one by the duplication of the corresponding knot. As a consequence, a weak discontinuity ($\mathcal{C}^0$) can be created by repeating a knot p times, and a strong discontinuity ($\mathcal{C}^{-1}$) by repeating it $p+1$ times (Figure 2). We refer to [31] for a complete overview of the properties of B-splines, and to [34] for a detailed discussion of the properties of interest in the context of poroelasticity.

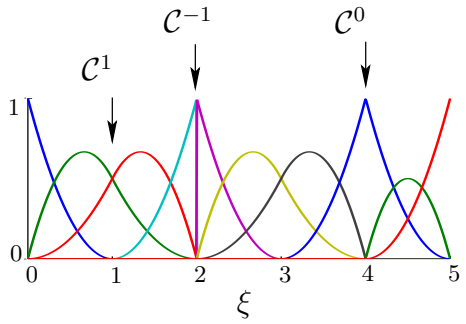

Figure 2. Second-order B-spline basis functions defined over the knot vector $\Xi = \{0, 0, 0, 1, 2, 2, 2, 3, 4, 4, 5, 5, 5\}$, where the knot value of 2 is repeated three times to make the basis discontinuous across the corresponding element boundary.

B-spline surfaces and volumes, referred to as patches, are constructed as tensor products of univariate B-splines. A surface patch, for example, is defined by the knot vectors $\Xi = \{\xi_1, \xi_2, \cdots, \xi_{n_\xi + p_\xi + 1}\}$ and $\mathcal{H} = \{\eta_1, \eta_2, \cdots, \eta_{n_\eta + p_\eta + 1}\}$, over which the sets of basis functions $\{N^{\xi}_{i,p_\xi}(\xi)\}_{i=1}^{n_\xi}$ and $\{N^{\eta}_{i,p_\eta}(\eta)\}_{i=1}^{n_\eta}$ are defined, respectively. Using a tensor product structure, $n = n_\xi n_\eta$ bivariate basis functions are then defined as

$$N_i(\boldsymbol{\xi}) = N^{\xi}_{\imath}(\xi) N^{\eta}_{\jmath}(\eta) \qquad \text{with } i = \imath + (\jmath - 1) n_\xi \text{ and } \boldsymbol{\xi} = (\xi, \eta). \tag{14}$$

[†]As is common in finite element literature, the terms 'order' and 'degree' are used synonymously in this manuscript. It is noted that in computer graphics literature it is common to define the order of a B-spline as the polynomial degree of the curve plus one.

DOI: 10.1002/nme

Note that the subscripts p, p_ξ and p_η have been dropped for notational convenience. In the remainder of this work we will consider equal orders in both parametric directions, i.e. $p_\xi = p_\eta = p$. The order p will be clear from the context. The set of control points, $\{\boldsymbol{X}_i \in \mathbb{R}^{n_d}\}_{i=1}^{n}$, associated with the multivariate basis functions (14) is referred to as the control net.

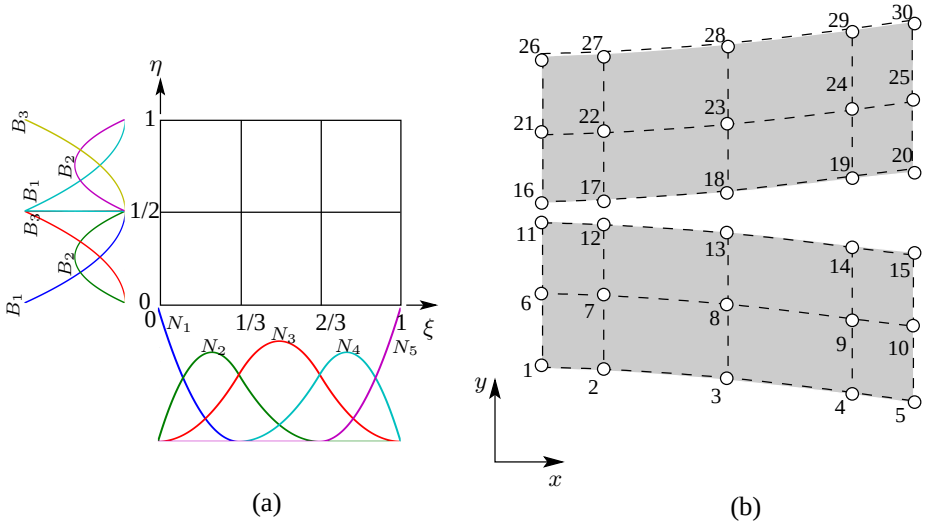

Figure 3. The parameter domain and control net for a mode-I delamination test of a double cantilever beam. (a) The parameter domain is partitioned by the global knot vectors $\Xi = \{0, 0, 0, \frac{1}{3}, \frac{2}{3}, 1, 1, 1\}$ and $\mathcal{H} = \{0, 0, 0, \frac{1}{2}, \frac{1}{2}, \frac{1}{2}, 1, 1, 1\}$. The interface is inserted through the repeated knot value at $\eta = \frac{1}{2}$. The bivariate basis functions for the B-spline patch are constructed as the tensor product of the univariate basis functions in each parametric direction. (b) The control net defines the physical domain through the isoparametric map. The discontinuity in the η-direction permits the creation of discontinuities in the geometry.

The tensor product structure of B-spline surfaces and volumes allows for the creation of discrete cracks by repeating a knot value in one of the tensorial directions $p + 1$ times. The resulting discontinuity in the univariate basis is then propagated throughout the complete specimen by virtue of the tensor product structure of B-splines. Evidently, this concept can be used directly to mimic adhesive layers that run throughout the entire domain. To localise the discontinuity and make the same strategy suitable for modelling propagating interfaces T-splines can be used [24]. In Figure 3 we show an example of a B-spline surface with a discontinuity inserted in a single tensorial direction.

3.2. The Bézier mesh

Over the past few years it has been shown that the spline bases underlying isogeometric analysis can be incorporated in standard finite element tools using Bézier extraction [25]. The idea of Bézier extraction is to represent the B-spline basis functions as element-wise polynomials. In this respect, the only difference between isogeometric analysis and traditional finite element is that the basis functions in isogeometric analysis are generally different per element. However, the element-specific basis functions, $\boldsymbol{N}^e$, can be constructed using a canonical set of polynomial element basis functions, $\boldsymbol{\mathcal{B}}$, by means of a linear transformation:

$$\boldsymbol{N}^e = \boldsymbol{C}^e \boldsymbol{\mathcal{B}} \tag{15}$$

The element-specific transformation matrix, $\boldsymbol{C}^e$, is referred to as the Bézier extraction operator. For the canonical set of basis function, $\boldsymbol{\mathcal{B}}$, in principle any basis for the polynomial space of the same order as the B-spline can be used. A natural choice in the context of isogeometric analysis is to use the Bernstein polynomials. We refer to [25] for a detailed discussion on the construction of the

DOI: 10.1002/nme

```
<Control_Points>
  1   0.0  0.0;
  2   1.0  0.0;
  .   ...
  .   ...
  30  6.0  2.0;

<Connectivity>
  1  'Bulk' 1   2   3   6   7   8   11  12  13;
  2  'Bulk' 2   3   4   7   8   9   12  13  14;
  .   ...
  .   ...
  6  'Bulk' 18  19  20  23  24  25  28  29  30;

<Extraction_Operators>
  1  [[ 1.0  0.0  0.0  0.0  0.0  0.0  0.0  0.0  0.0 ],
     [ 0.0  1.0  0.5  0.0  0.0  0.0  0.0  0.0  0.0 ],
     [ 0.0  0.0  0.5  0.0  0.0  0.0  0.0  0.0  0.0 ],
     [ 0.0  0.0  0.0  1.0  0.0  0.0  0.0  0.0  0.0 ],
     [ 0.0  0.0  0.0  0.0  1.0  0.5  0.0  0.0  0.0 ],
     [ 0.0  0.0  0.0  0.0  0.0  0.5  0.0  0.0  0.0 ],
     [ 0.0  0.0  0.0  0.0  0.0  0.0  1.0  0.0  0.0 ],
     [ 0.0  0.0  0.0  0.0  0.0  0.0  0.0  1.0  0.5 ],
     [ 0.0  0.0  0.0  0.0  0.0  0.0  0.0  0.0  0.5 ]];
  .   ...
  .   ...
  6  [[ ...
     [ ... ]];
```

Figure 4. Mesh file for the bulk part of the double cantilever beam of Figure 3. The coordinates of the control points are given after the label `<Control_Points>`. The control point ID number is given first, followed by the x- and y-coordinate of the point. The element connectivity is given next. In this case, each bulk element is supported by 9 control points. Finally, the extraction operator matrix for each of the 6 elements is given. The dimension of these matrices is $[9 \times 9]$ and they are generally sparse. In this example, the full matrices are stored. In order to reduce the length of the input file, one can use a sparse format instead.

extraction operators for B-spline patches. Note that, from the perspective of implementation, the element extraction operators are implemented at the level of basis function evaluations, and hence do not need to appear in the model-specific parts of a finite element implementation. In this way, we can utilize the spline functions without changing the model.

Using Bézier extraction a finite element data structure for splines can be constructed. An example of this data structure, referred to as the Bézier mesh, is shown in Figure 4. For the continuum domain, the Bézier mesh consists of a set of control points, a connectivity table (`IEN`-array) in which the control points are listed that support a given element, and the element extraction operators [25]. In Figure 4 the extraction operators are represented by full matrices. In practice, the sparsity of the operators is exploited to reduce the size of the mesh files. Moreover, the fact that the extraction operators coincide for many elements can be exploited. We illustrate the Bézier extraction concept in Figure 5 for the B-spline patch introduced in Figure 3. Note that the discontinuous basis is fully represented by the Bézier extraction.

3.3. The Bézier interface element

In this contribution we demonstrate how the Bézier extraction concept can be used to provide a finite element data structure for isogeometric interface elements. Similar to the interface elements used in traditional finite element models, an interface element in isogeometric analysis essentially provides an interpolation of the jump in the field variables over an interface. As indicated in the previous section, an interface in a B-spline patch is created by increasing the multiplicity of a knot in one

DOI: 10.1002/nme

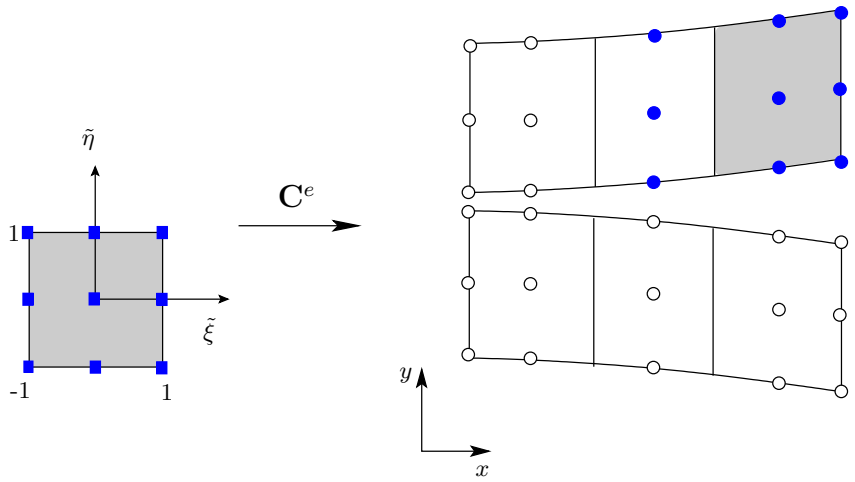

Figure 5. The Bézier continuum element consists of a set of basis functions defined over a parent element, which are mapped to the physical domain by means of an isoparametric map. It is noted in this paper that the Bézier mesh is denoted in solid line, while the control net is denoted in dash line, as described previously on Figure 3.

of the parametric directions. This interface is then parametrised by a lower dimensional spline (a univariate spline in two dimensions or a bivariate spline in three dimensions).

As for the basis functions over the bulk material, the interface basis functions can also be constructed using Bézier extraction. Again the idea is to map a canonical set of basis functions defined over a parent element to a set of element-specific B-spline basis functions, see Figure 6. The interface extraction operators can either be constructed directly from the univariate knot vector in the direction of the interface, or be inherited from the extraction operators of the neighbouring bulk elements. A fundamental difference between a standard line element and an interface element is that the interface element is connected to the surrounding bulk elements on two sides. Since the isogeometric interface element is an isoparametric element, the consequence of this two-side connectivity is that the geometry definition can be ambiguous. In the case that the geometry is merely described in the undeformed configuration, the interface control points can be taken as the control points on the boundary of the bulk material on either side of the crack (e.g. points 1–3 in Figure 6). In the case of large deformations a common assumption is to use the average of the control points on the two sides of an interface, see e.g. [16].

The isogeometric interface extraction for the B-spline patch in Figure 3 is shown schematically in Figure 7. The finite element data structure for the interface element is shown in Figure 8. The control points remain unaltered compared to the case of a bulk mesh, since the interface is fully defined by the bulk control points. The control point numbers on either side of the interface are collected in the connectivity table. Although it is possible that only the control points on one side of the interface are used for the geometry parametrisation, it is an essential feature of the interface element to couple the field variables on either side of the interface. The operations required to interpolate the jump in the field variables over the interface are discussed in detail in Section 4.

4. WEAK FORM AND DISCRETISATION

A Bézier interface element is obtained by discretising the internal boundary term of the linear momentum equation are discretised using B-splines and the aforementioned Bézier extraction technique. In addition, a concise derivation of a poromechanical Bézier interface element is given.

DOI: 10.1002/nme

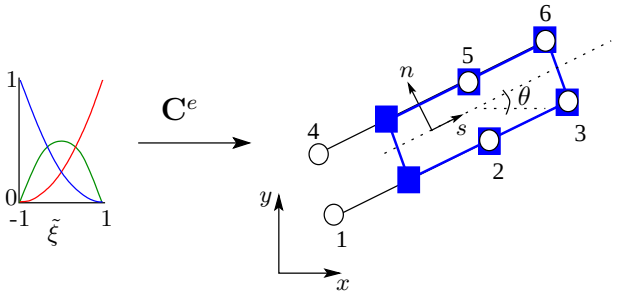

Figure 6. The Bézier interface element consists of a set of basis functions defined over a parent element, which are mapped to the physical domain by means of an isoparametric map. The interface element connects the continuum basis functions on both sides of the interface. The ◯'s indicate the control points which influence the location of Bézier points, indicated by ■'s.

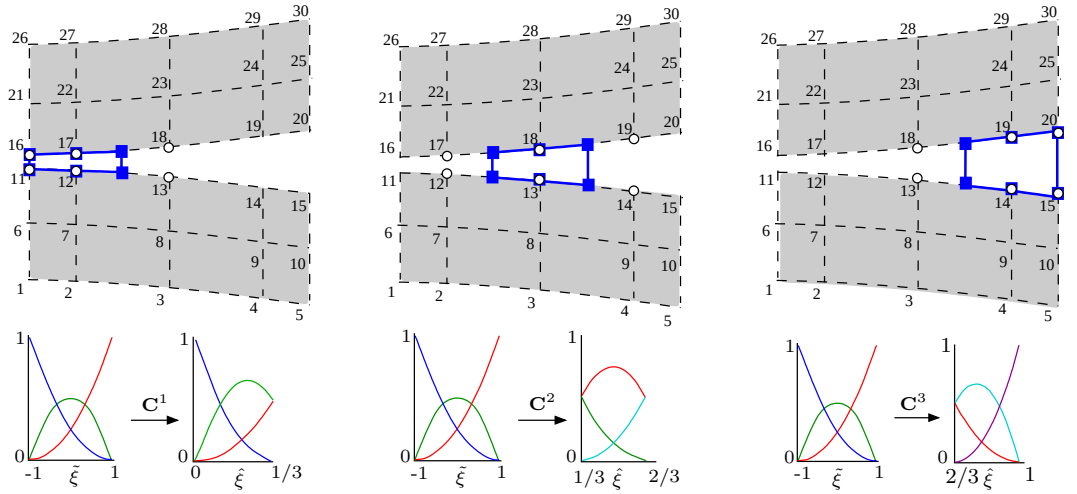

Figure 7. The deformed state of quadratic Bézier interface elements under mode-I loading condition, denoted by the blue lines. For each element e the ◯'s indicate the control points which influence the location of Bézier points, indicated by ■'s. The Bézier extraction operator $\boldsymbol{C}^e, e = 1, 2, 3$, maps a canonical set of element functions, defined over the parent element, onto the element-specific basis functions $\boldsymbol{N}^e$

4.1. Discretisation of the linear momentum equation

The derivation of the interface element follows the same steps as the derivation of a classical interface element as presented by Schellekens and de Borst [2]. The weak form of the balance equation is obtained by multiplication of the linear momentum equation (1) with an admissible displacement field $\delta\mathbf{u}$ and integrating over the product over the domain Ω:

$$\int_\Omega \delta\mathbf{u} \cdot \nabla\boldsymbol{\sigma} \mathrm{d}\Omega = 0 \tag{16}$$

Applying Gauss theorem, using the symmetry of the Cauchy stress tensor, introducing the internal boundary Γ_d and the corresponding admissible interface opening $\delta\mathbf{v}$, and using the boundary conditions at the external boundary Γ_t gives: the product over

$$\int_\Omega \nabla\delta\mathbf{u} : \boldsymbol{\sigma} \, \mathrm{d}\Omega + \int_{\Gamma_\mathrm{d}} \delta\mathbf{v} \cdot \mathbf{t} \, \mathrm{d}\Gamma = \int_{\Gamma_t} \delta\mathbf{u} \cdot \bar{\mathbf{t}} \, \mathrm{d}\Gamma \tag{17}$$

DOI: 10.1002/nme

```
<Connectivity>
  7  'Interface' 11  12  13  16  17  18;
  8  'Interface' 12  13  14  17  18  19;
  9  'Interface' 13  14  15  18  19  20;

<Extraction_Operators>
  7 [[ 1.0  0.0  0.0 ],
     [ 0.0  1.0  0.5 ],
     [ 0.0  0.0  0.5 ]];
  8 [[ 0.5  0.0  0.0 ],
     [ 0.5  1.0  0.5 ],
     [ 0.0  0.0  0.5 ]];
  9 [[ 0.5  0.0  0.0 ],
     [ 0.5  1.0  0.0 ],
     [ 0.0  0.0  0.1 ]];
```

Figure 8. Mesh file for the interface elements of the double cantilever beam of Figure 3. The interface elements are supported by six control points, which have been defined in Figure 4. The extraction operator matrices have the dimensions $[3 \times 3]$

.

The first term of this equation is the weak form of the linear momentum of the bulk material. The last term represents the external, distributed load, see Reference [34]. In the remainder of this section, we will confine attention to the derivation of the Bézier elements of the second term of Equation (17), the cohesive interface.

The interface is represented as a discontinuity in the mesh. In a discrete sense, it consists of adjacent planes (or lines in a two-dimensional system) which are connected to the bulk elements, see Figure 6. Each plane has its own displacement field: the displacement of the plane that is associated to the Ω^+ part of the domain is denoted by $\mathbf{u}^+$, and the continuous displacement field of the plane associated to the Ω^- part of the domain, is denoted by $\mathbf{u}^-$. Both displacement fields can be approximated in terms of the same, element-specific B-spline basis functions of a given element e, $\mathbf{N}_i^e(\xi)$, according to

$$\mathbf{u}^+ = \sum_{i=1}^{n^e} N_i^e(\xi)\mathbf{a}_{i+n^e}^e \; ; \qquad \mathbf{u}^- = \sum_{i=1}^{n^e} N_i^e(\xi)\mathbf{a}_i^e \tag{18}$$

where ξ is the parametric coordinate, n^e is the number of control points i that construct a single face of element e and $\mathbf{a}_i^e$ are the discrete displacements in these control points. In the case of a quadratic Bézier element, as depicted in Figure 6, n_e is equal to 3. Note that an interface element consists of two faces and therefore the total number of control points equals $2n_e$.

The opening of the interface $\mathbf{v}$ is defined as the relative displacement of a point ξ on both faces of the element:

$$\mathbf{v}(\xi) = \mathbf{u}^+(\xi) - \mathbf{u}^-(\xi) \tag{19}$$

In the discrete version, this can be written as:

$$\mathbf{v}(\xi) = \mathbf{H}(\xi)\mathbf{a} \tag{20}$$

The matrix $\mathbf{H}(\xi)$ that maps the discrete displacements of the control points to the interface opening contains the element interpolation functions. In the case of a two-dimensional element this matrix has dimensions $[2 \times 4n^e]$ and is structured as follows:

$$\mathbf{H}(\xi) = \begin{bmatrix} -N_1^e & 0 & -N_2^e & 0 & \dots & -N_{n^e}^e & 0 & N_1^e & 0 & \dots & N_{n^e}^e & 0 \\ 0 & -N_1^e & 0 & -N_2^e & \dots & 0 & -N_{n^e}^e & 0 & N_1^e & \dots & 0 & N_{n^e}^e \end{bmatrix} \tag{21}$$

For the sake of brevity, the dependence on ξ has been dropped in the matrix description above. The opening of the interface element $\mathbf{v}$ is transformed to the interface local frame of reference using

DOI: 10.1002/nme

Equation (4). In conventional interface elements, the rotation matrix $\mathbf{R}$ is assumed to be constant over the element and is constructed by evaluating the nodal positions of the element, see [2]. In the case of Bézier elements, it is possible to construct a unique rotation matrix for each material point of the element by using the continuous displacement fields.

To this end, we describe the position of the mid-surface of the interface element, denoted by the dashed line in Figure 1, in the deformed configuration

$$\mathbf{x}_{\mathrm{d}}(\xi) = \mathbf{X}_{\mathrm{d}}(\xi) + \frac{1}{2}\left(\mathbf{u}^{+}(\xi) + \mathbf{u}^{-}(\xi)\right) \tag{22}$$

The tangential vector $\mathbf{s}_{\Gamma_{\mathrm{d}}}$ in this point is equal to the derivative of the spatial position with respect to the isoparametric coordinate ξ:

$$\mathbf{s}_{\Gamma_{\mathrm{d}}}(\xi) = \frac{\frac{\partial \mathbf{x}_{\mathrm{d}}}{\partial \xi}}{||\frac{\partial \mathbf{x}_{\mathrm{d}}}{\partial \xi}||} \tag{23}$$

The normal vector $\mathbf{n}_{\Gamma_{\mathrm{d}}}$ is perpendicular to this vector, $\mathbf{n}_{\Gamma_{\mathrm{d}}} \cdot \mathbf{s}_{\Gamma_{\mathrm{d}}} = 0$ in the case of a two-dimensional implementation. Finally, the rotation matrix is equal to:

$$\mathbf{R} = \left[\mathbf{n}_{\Gamma_{\mathrm{d}}}^{T}, \mathbf{s}_{\Gamma_{\mathrm{d}}}^{T}\right] \tag{24}$$

Introducing the rotation matrix in the discretised interface internal force vector $\mathbf{f}_{\Gamma_{\mathrm{d}}}^{\mathrm{int}}$ yields:

$$\mathbf{f}_{\Gamma_{\mathrm{d}}}^{\mathrm{int}} = \int_{\Gamma_{\mathrm{d}}} \mathbf{R}^{\mathrm{T}}\mathbf{H}^{\mathrm{T}}\mathbf{t}_{\mathrm{d}}\mathrm{d}\Gamma \tag{25}$$

Straightforward linearisation of this equation gives:

$$\mathbf{K}_{\Gamma_{\mathrm{d}}} = \int_{\Gamma_{\mathrm{d}}} \mathbf{R}^{\mathrm{T}}\mathbf{H}^{\mathrm{T}}\mathbf{T}_{\mathrm{d}}\mathbf{H}\mathbf{R}\mathrm{d}\Gamma \tag{26}$$

where the higher order terms that contain the derivatives of the rotation matrix $\mathbf{R}$ with respect to the displacements have been omitted at the expense of a slightly slower convergence. The matrix $\mathbf{T}_{\mathrm{d}}$ is the consistent tangent of the cohesive constitutive law in the interface local frame of reference, as defined in Equation (3).

4.2. Numerical integration

The spatial numerical integration is an important issue in conventional interface elements when applied in the context of cohesive surface models. They can suffer from spurious traction oscillations, in particular in quasi-brittle fracture where there is no compliant interface prior to reaching the tensile strength. The magnitude of these oscillations increases with an increasing dummy stiffness, which is used prior to the opening of the discontinuity in order to ensure continuity [6]. A solution that is generally accepted is to abandon Gauss integration of the interface element and to resort to Newton-Cotes integration or to lumped integration techniques. This approach suppresses the oscillations in classical zero-thickness interface elements [2], but also in thin layer interface formulations such as in the cohesive band method [35].

We now investigate whether the Bézier interface elements inherit this deficiency. For this purpose, we employ a notched three-point bending beam, shown in Figure 9, and used before in Reference [2]. The dimensions of the beam are $w = 125\,\mathrm{mm}$ and $h = 100\,\mathrm{mm}$, and is made of an elastic, isotropic material with Young's modulus $E = 20\,000\,\mathrm{MPa}$ and a Poisson's ratio $\nu = 0.2$. The length of the notch is $a = 20\,\mathrm{mm}$. The applied external load is equal to $P = 1000\,\mathrm{N}$.

The model consists of a patch of 64×16 cubic Bézier elements. The interface is represented by Bézier interface elements. The notch, located at $0 < y < 20\,\mathrm{mm}$, is traction free. Here, the tractions $\mathbf{t}_{\mathrm{d}}$ and the tangent stiffness matrix $\mathbf{T}_{\mathrm{d}}$ vanish, irrespective of the magnitude of the strain field. At the interface, i.e. when $20 < y < 100\,\mathrm{mm}$, an elastic 'dummy' stiffness constitutive relation is used. The location of this region is determined by assigning a dummy stiffness with a magnitude that is

DOI: 10.1002/nme

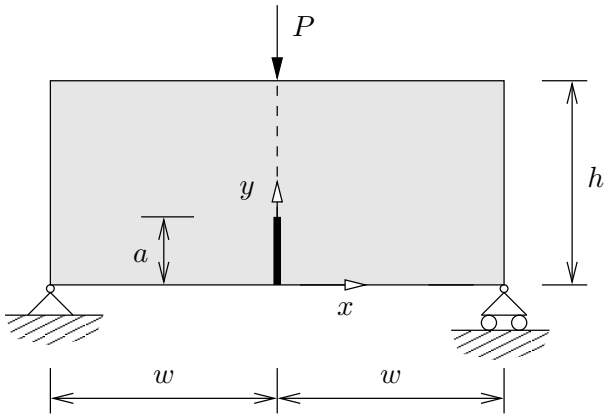

Figure 9. Geometry and boundary conditions of a notched beam in a three-point bending test

based on the spatial position of the corresponding integration point. Hence, the interface stiffness is represented by the following cohesive relation:

$$\mathbf{t}_{\mathrm{d}} = \mathbf{T}_{\mathrm{d}}\mathbf{v}_{\mathrm{d}} \qquad \text{where } \mathbf{T}_{\mathrm{d}} = \mathrm{diag}(D, D) \qquad \text{where } D = \begin{cases} 0 & \forall\, y < 20 \\ D & \forall\, y \geq 20 \end{cases} \tag{27}$$

Calculations have been carried out for different magnitudes of the dummy stiffness D. The spatial integration along the interface is done using either Gauss or Newton-Cotes integration. The traction profiles at the interface are shown in Figures 10 and 11.

The results for the Bézier interface element confirm those obtained for a classical interface element [2] in the sense that traction oscillations are present when a Gauss integration scheme is used, and increase for larger values of the dummy stiffness D. As a result of the higher order interelement continuitiy of spline functions the oscillations do not disappear when a Newton-Cotes integration scheme is used, see Figure 11.

4.3. Poromechanical interface

One of the advantages of using isogeometric interpolation fields is the existence of higher order derivatives of the shape functions. This allows to capture the Darcy flow in Equation (10) exactly, instead of enforcing the higher order derivatives in a weak sense only [23].

The extension towards a poromechanical interface element is straightforward. Similar to the linear momentum equation, the mass balance equation (5) is multiplied by the admissible pressure field δp:

$$\int_{\Omega} \delta p \alpha \nabla \cdot \dot{\mathbf{u}}\, \mathrm{d}\Omega + \int_{\Omega} \delta p \frac{1}{M} \dot{p}_{\mathrm{f}}\, \mathrm{d}\Omega + \int_{\Omega} \delta p \nabla \cdot \mathbf{q}\, \mathrm{d}\Omega = 0 \tag{28}$$

Applying Gauss' theorem and introducing Darcy's relation (7), this equation can be rewritten as:

$$-\int_{\Omega} \delta p \alpha \nabla \cdot \dot{\mathbf{u}}\, \mathrm{d}\Omega - \int_{\Omega} \delta p \frac{1}{M} \dot{p}_{\mathrm{f}}\, \mathrm{d}\Omega + \int_{\Omega} \nabla \delta p \cdot \frac{k}{\mu} \nabla p_{\mathrm{f}}\, \mathrm{d}\Omega + \int_{\Gamma_{\mathrm{d}}} \delta p \mathbf{n}_{\Gamma_{\mathrm{d}}} \cdot \mathbf{q}\, \mathrm{d}\Gamma = \int_{\Gamma_q} \delta p \mathbf{n} \cdot \mathbf{q}\, \mathrm{d}\Gamma \tag{29}$$

Herein, we focus on the discretisation of the mass balance term for the interface, the fourth term in the left hand side of this equation. The discretisation of the other terms using a Bézier extraction technique has been discussed in detail in Reference [34].

The discrete pressure field in the discontinuity is equal to:

$$p_{\mathrm{f}} = \sum_{i=1}^{n_e} N_i^e b_i^e \tag{30}$$

DOI: 10.1002/nme

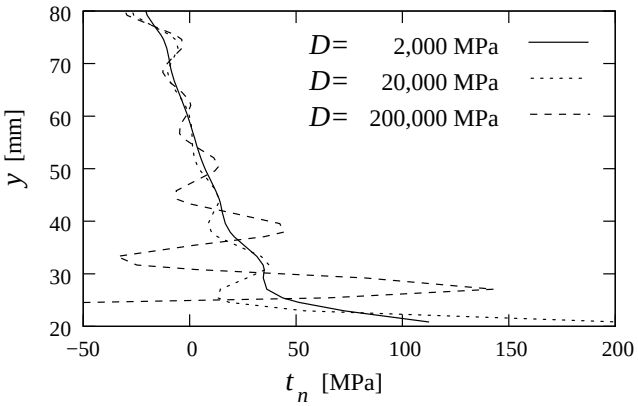

(a) Bézier interface elements

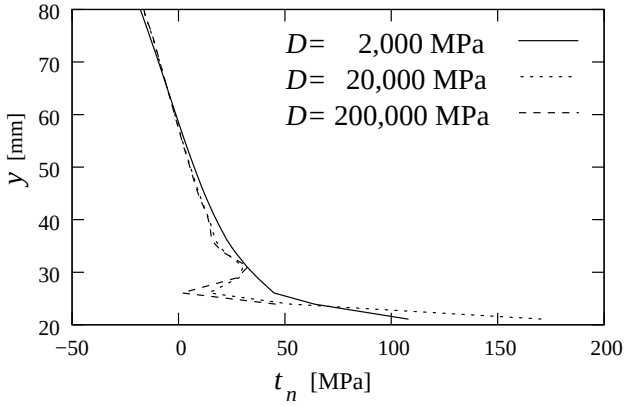

(b) Standard interface elements

Figure 10. Interface traction t_n as a function of the position at the interface for different magnitudes of the dummy stiffness D for a Gauss integration scheme.

where b_i^e are the nodal discrete pressures at the face of the interface element associated with the Ω^- part of the domain. The pressure is weakly discontinuous at the interface. Therefore, the pressure degrees of freedom associated with the top surfaces are constrained to those on the bottom surface, such that the pressure in a specific material point on the surface associated with Ω^+ is identical to that in the corresponding material point on the Ω^- surface. As a result, the pressure p_f can be discretised using the pressures b_i at the knots that support the Ω^- surface only:

$$p_\mathrm{f} = \mathbf{N}\mathbf{b} \tag{31}$$

where $\mathbf{N}$ is

$$\mathbf{N} = [N_1^e, N_2^e, ..., N_{n^e}^e] \tag{32}$$

Similar to the linear momentum equation, we adopt a Bubnov-Galerkin formulation. Hence, inserting the variation of the discretised pressure into the interface term of the weak forms as described in Equation (29) yields:

$$\mathbf{q}_{\Gamma_\mathrm{d}}^{\mathrm{int}} = \int_{\Gamma_\mathrm{d}} \mathbf{N}^\mathrm{T} \mathbf{n}_{\Gamma_\mathrm{d}}^\mathrm{T} \mathbf{q} \, \mathrm{d}\Gamma. \tag{33}$$

This interfacial flux vector $\mathbf{q}_{\Gamma_\mathrm{d}}^{\mathrm{int}}$ can subsequently be elaborated in a similar manner to that in Reference [22]. The time integration is carried out using a backward Euler finite difference scheme, similar to [19] and [34]. The non-linear system of equations is solved using a Newton-Raphson procedure.

DOI: 10.1002/nme

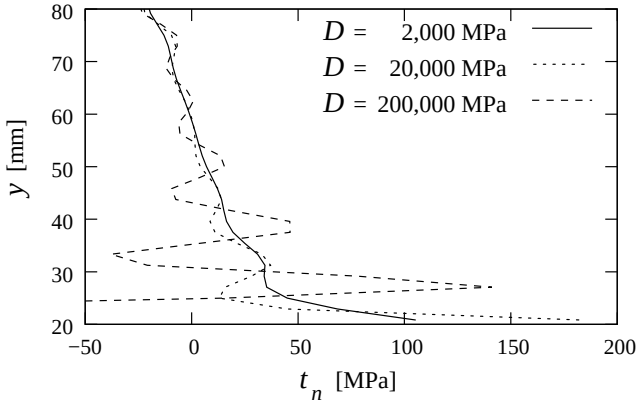

(a) Bézier interface elements

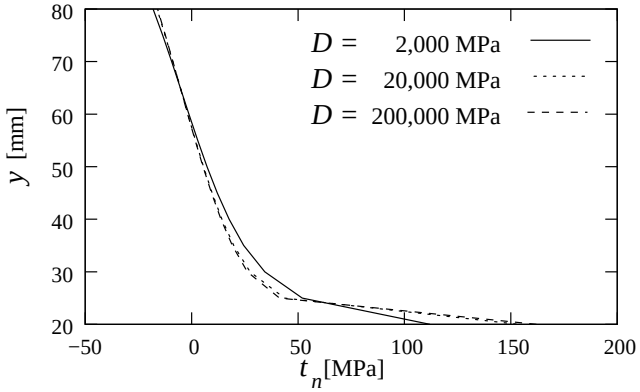

(b) Standard interface elements

Figure 11. Interface traction t_n as a function of the position at the interface for different magnitudes of the dummy stiffness D for a Newton Cotes integration scheme.

5. NUMERICAL EXAMPLES

To illustrate the wide range of problems that can be solved by the present approach, we simulate some crack propagation problems in porous and non-porous media. The first example shows the robustness and the accuracy of the discretisation method for modeling crack propagation in a standard solid medium. The second example illustrates its capability to analyse deformation and flow in a cracked, fully saturated porous medium. The third example focuses on crack propagation in a porous medium, taking into account the fluid flow inside the crack.

5.1. Double cantilever beam

We consider the double cantilever beam shown in Figure 12. The beam has a length $l = 10$ mm and a thickness $h = 0.5$ mm. It is composed of an elastic material with a Young's modulus $E = 100$ MPa and a Poisson's ratio $\nu = 0.3$. The beams are bonded by an adhesive with a strength $f_t = 1.0$ MPa and a toughness $\mathcal{G}_c = 0.1$ N/mm. The interface is modelled with a Xu-Needleman cohesive relation [8]. The length of the initial delamination is $a = 1$ mm. Mesh convergence studies have been carried out for meshes with 16×2, 32×4, 64×8 and 128×16 linear rectangular finite elements and for quadratic and cubic Bézier elements.

The load displacement curve is given in Figure 13 for cubic Bézier elements, which shows that the converged solution is achieved for relatively coarse meshes of cubic Bézier elements. The mesh sensitivity analyses are shown in Figure 14, in which the load P at a displacement $u = 2$ mm is compared for various mesh size and for various degrees of interpolation of the Bézier interface

DOI: 10.1002/nme

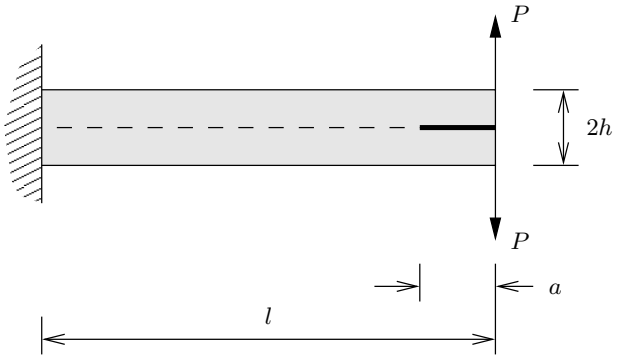

Figure 12. Geometry of DCB Test

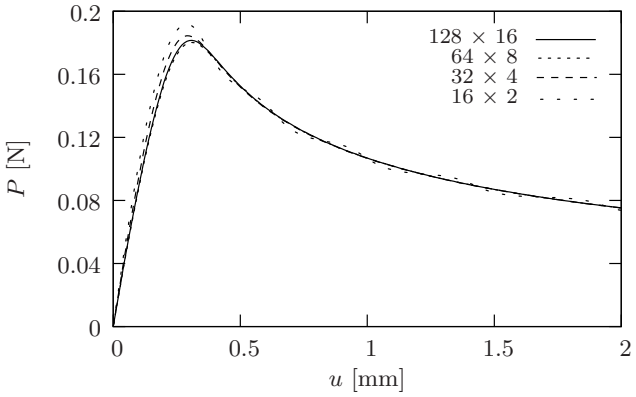

Figure 13. Load-displacement curve for the double cantilever beam. Cubic Bézier interface elements have been used with different levels of mesh refinement.

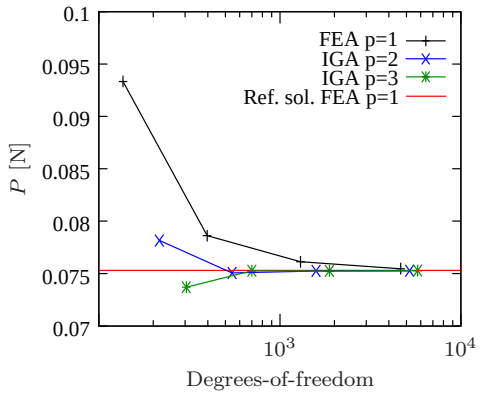

Figure 14. Mesh sensitivity analyses for the double cantilever beam. The load P at a displacement $u = 2$ mm is compared for various levels of mesh refinement and for various degrees of interpolation of standard and Bézier interface elements. The reference solution has been computed for a dense finite element mesh with 33924 degrees of freedom.

elements and for standard interface elements. The results are compared with a reference solution generated by a dense finite element mesh with 33924 degrees of freedom. From Figure 14 it is observed that the results of the Bézier interface elements converge faster to the reference solution and, moreover, result in a smooth traction profile along the interface, see Figure 15.

DOI: 10.1002/nme

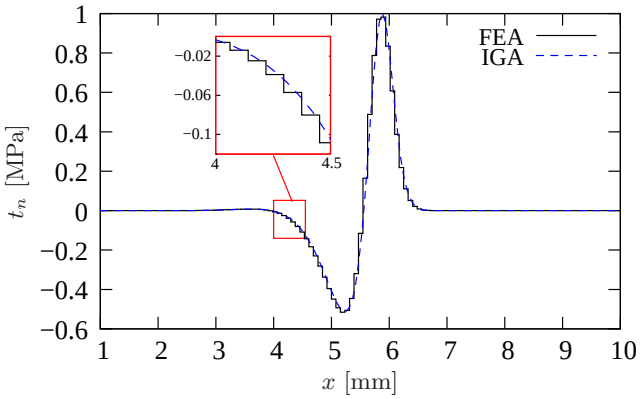

Figure 15. A comparison of the traction profiles between standard linear interface elements (4464 degrees of freedom) and cubic Bézier interface elements (1876 degrees of freedom) for a displacement $u = 2$ mm.

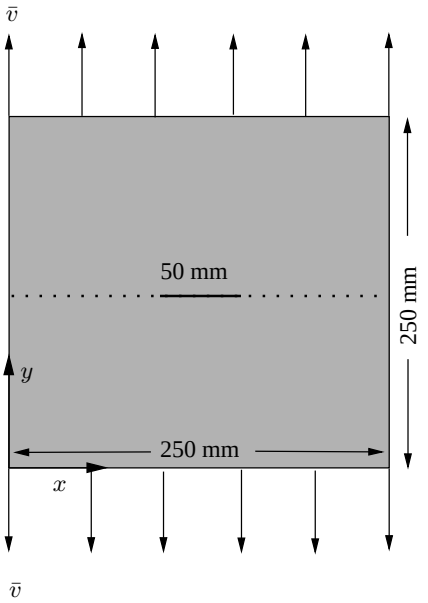

Figure 16. A square block of a fluid-saturated porous material with an initial crack.

5.2. Traction-free crack

Next, a square block of a fluid-saturated porous material is subjected to pure mode-I loading, Figure 16. The material has a Young's modulus $E = 25.85\,\text{GPa}$, a Poisson's ratio $\nu = 0.18$, a porosity $\phi = 0.2$, an intrinsic permeability $k = 2.78 \times 10^{-13}\,\text{mm}^2$ and a fluid viscosity $\mu = 5 \times 10^{-10}\,\text{MPa s}$. The bulk modulus of the solid material $K_s = 13.46\,\text{GPa}$, while for the fluid $K_f = 2.3\,\text{GPa}$. The Biot coefficient has been assumed as $\alpha = 1$. A velocity $\bar{u} = 5. \times 10^{-3}\text{mm/s}$ has been applied at the top and the bottom sides of the block, and a time step $\Delta t = 1\,\text{s}$ has been used.

The problem has been discretised using rectangular Bézier elements and Bézier interface elements with cubic B-spline basis functions. The mesh incorporates interfaces elements at $y = 125$ mm. The centre 50 millimeters of the discontinuity are traction free, representing a fully open crack, while at the remaining part a dummy stiffness $D = 10^3\,\text{N/mm}$ has been used to enforce no opening at the discontinuity line. Mesh convergence studies have been carried out and three levels of discretisation

DOI: 10.1002/nme

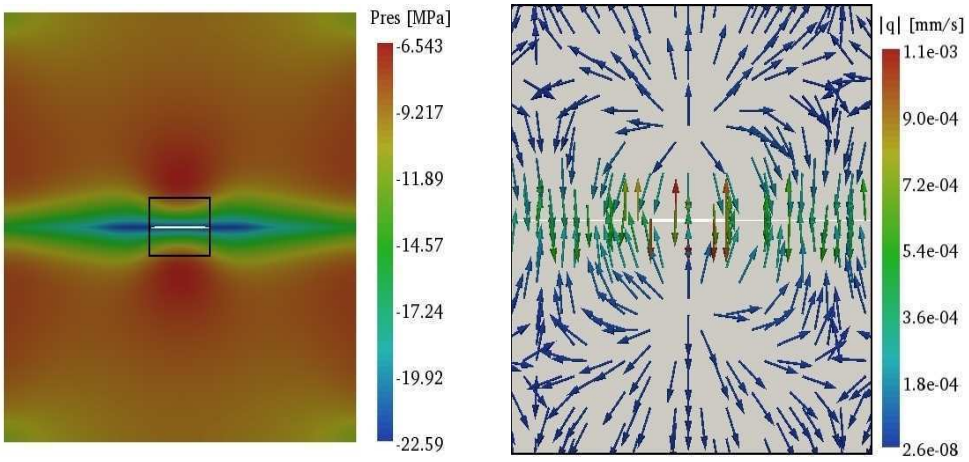

(a) Pressure profile (b) Fluid relative velocity profile

Figure 17. $t = 50\,\mathrm{s}$: (a) pressure profile; and (b) relative fluid velocities for the area enclosed by the black square box of (a).

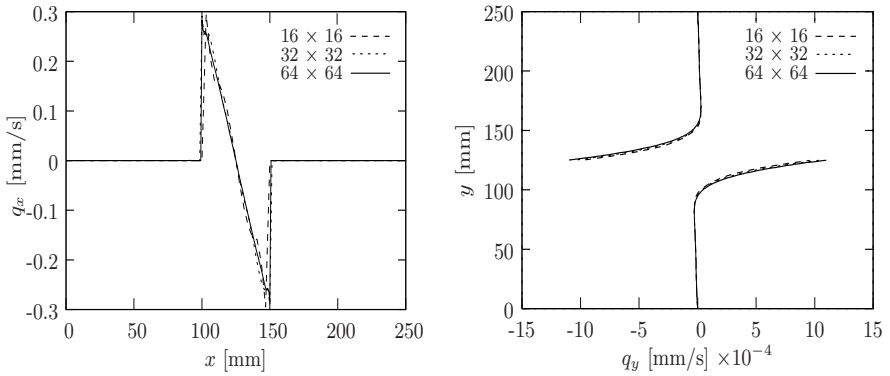

(a) Relative fluid velocity tangential to the crack (b) Relative fluid velocity normal to the crack

Figure 18. Mesh sensitivity analysis for the cubic Bézier elements

have been considered, namely 16×16, 32×32 and 64×64 cubic Bézier elements, resulting in 1254, 3990 and 14070 degrees of freedom, respectively.

Figure 17(a) shows the pressure profile of the block at $t = 50\,\mathrm{s}$. At the crack tip a high suction appears, which significantly affects the fluid flow. Indeed, Figure 17(b) shows that the fluid flow is sucked into the crack, and primarily at its tip. The relative fluid velocity in the direction tangential to the crack has been plotted in Figure 18(a). The fluid flows from the tip to the centre of the crack with a velocity that depends on the crack opening. The leakage from the surrounding porous medium is shown in Figure 18(b). The smooth flow profile is obtained by virtue of the smoothness of the spline functions.

5.3. Crack growth

The same setting as in Figure 16 has been used to analyse crack growth in a porous medium. A 50 millimeter long traction-free slit is inserted along the horizontal centre line of the specimen. A velocity $\bar{\dot{u}} = 5.0 \times 10^{-3}$ mm/s has been applied at the top and the bottom of the block until $t = 30$s. The displacement at the top and the bottom is then kept constant until $t = 500$s. A time step $\Delta t = 1\,\mathrm{s}$ has been used throughout.

DOI: 10.1002/nme

In the interface elements that are not used to model the initial traction-free slit, a dummy stiffness $D = 1 \times 10^3$ N/mm^2 has been inserted prior to the onset of cracking. After crack initiation at a tensile strength $f_t = 2.7$ MPa, a linear decohesion is applied with a fracture energy $\mathcal{G}_c = 0.05$ N/mm. Inside the crack a permeability has been assumed that equals that of the surrounding bulk prior to crack initation, while it increases progressively according to a cubic relation thereafter.

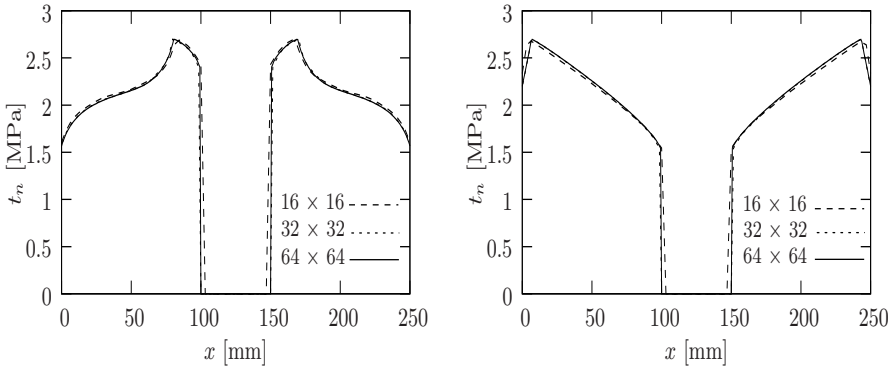

(a) Traction profile at $t = 30$ s (b) Traction profile at $t = 500$ s

Figure 19. Traction profiles for different levels of mesh refinement.

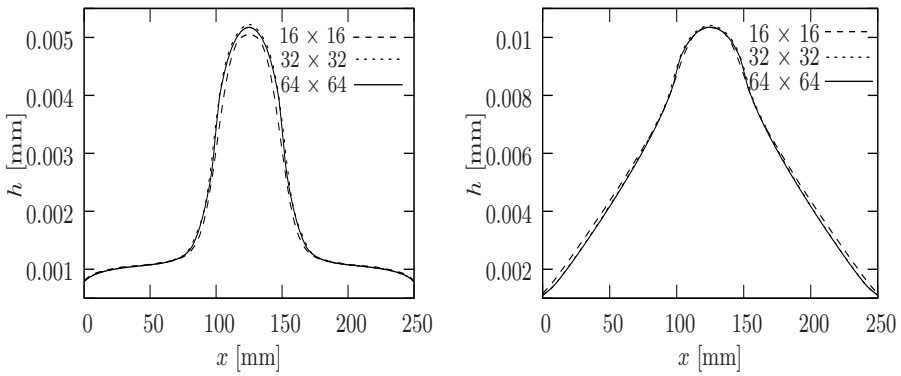

(a) Crack opening profiles at $t = 30$ s (b) Crack opening profiles at $t = 500$ s

Figure 20. Crack opening profiles for different levels of mesh refinement.

A mesh convergence analysis has been carried out using the same elements and for the same levels of mesh refinement as in the previous subsection. The results are shown in Figures 19 – 24, and in Table I. Figures 19 and 20 show the traction and the opening profiles for $t = 30$ s and $t = 500$ s, i.e., when the imposed displacement is kept constant. During this period, the redistribution of the fluid along the interface increases the stress at the crack tip. When the stress at the tip reaches the tensile strength f_t, the crack will propagate. Table I quantifies the mesh sensitivity for the point $(0, 125)$ mm and time $t = 30$ s, where the reference solution has been obtained using a dense mesh of cubic Bézier elements with 52662 degrees of freedom.

Figure 21 and 22 show the evolution of the the pressure and the relative fluid velocity profiles tangential to the interface during the period that the imposed displacement is kept constant. It is noted that due to fluid redistribution along the interface during this period the pressure at the interface decreases in absolute value. Since the gradient of the pressure along the crack also decreases, we observe the same effect on the relative fluid velocity along the crack. Contour plots of the pressure and the relative fluid velocity in the x-direction are given in Figures 23 and 24, respectively.

DOI: 10.1002/nme

	mesh	dofs	t_n [MPa]	% error	q_s[μm/s]	% error
p=3	16x16	1254	1.748	0.0051	9.49e-4	9.1967
p=3	32x32	3990	1.752	0.0028	3.37e-4	2.6186
p=3	64x64	14070	1.759	0.0011	1.92e-4	1.0673
Ref.	p=3, 128x128	52662	1.757	-	9.30e-5	-

Table I. Mesh sensitivity analyses for crack growth in porous medium at point $(0, 125)$ mm and time $t = 30$ s.

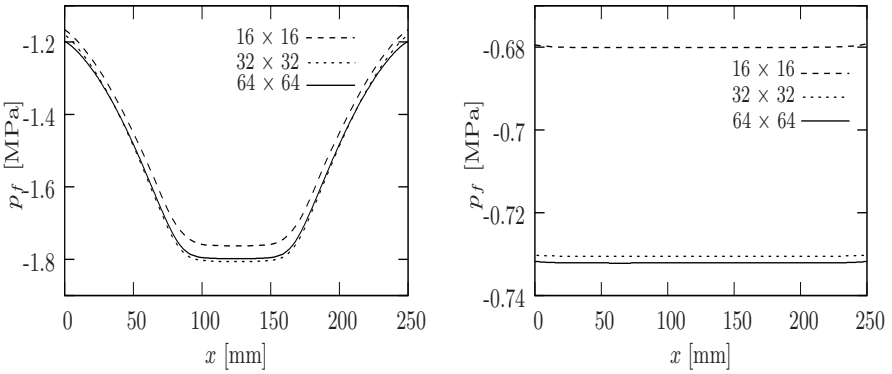

(a) Pressure profiles at $t = 30$ s (b) Pressure profiles at $t = 500$ s

Figure 21. Pressure profiles for different levels of mesh refinement.

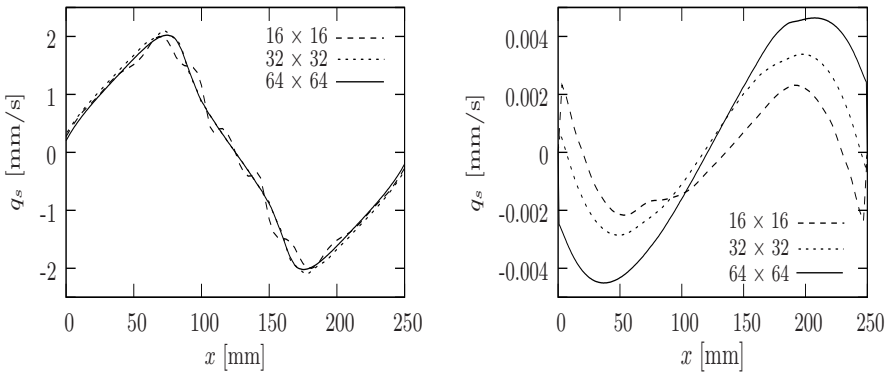

(a) Relative fluid velocity profiles at $t = 30$ s (b) Relative fluid velocity profiles at $t = 500$ s

Figure 22. Relative fluid velocity profiles along the crack for different levels of mesh refinement.

6. CONCLUDING REMARKS

An isogeometric interface element has been formulated. It exploits Bézier extraction, which makes it fully compatible with existing finite element software. Indeed, the current isogemetric interface element can be obtained by simply replacing the shape functions of conventional interface elements. Evidently, the shape functions are in principle now different for each interface element.

The new interface element shares all the advantages of isogeometric analysis, including the exact description of the geometry and the easy mesh generation. At the same time, it inherits properties from conventional interface elements such as the traction oscillations which occur when a very high (dummy) interface stiffness is used to suppress deformations in the interface prior to crack initiation. An examination of a beam subject to three-point bending suggests, however, that the higher smoothness of the spline functions used in isogeometric analysis prevents the decoupling

Prepared using nmeauth.cls
DOI: 10.1002/nme

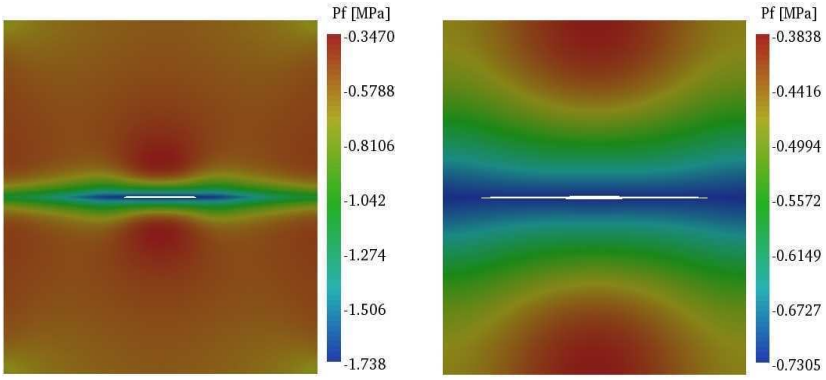

(a) (b)

Figure 23. Pressure contours at (a) $t = 30$ s and (b) $t = 500$s

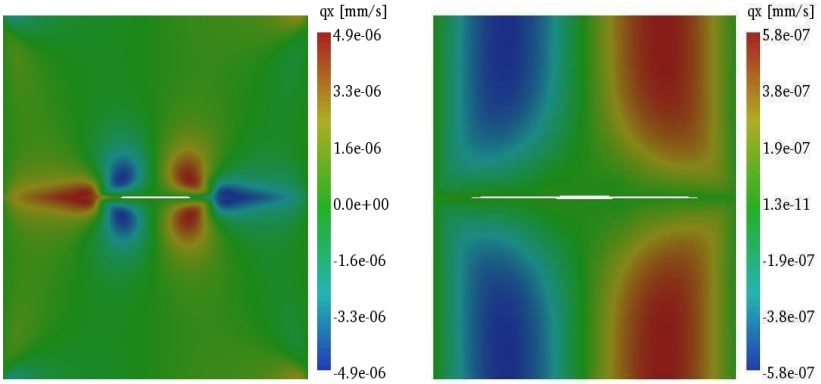

(a) (b)

Figure 24. Relative fluid velocity contours in the x-direction at (a) $t = 30$ s and (b) $t = 500$s

that is achieved using Newton-Cotes or nodal integration, which has proven a simple remedy for conventional interface elements [2].

In a previous paper [34] it has been shown that isogeometric finite elements also have advantages in poroelasticity, the natural preservation of the local mass balance being one of the most prominent. For this reason, the isogeometric interface element based on Bézier extraction has been extended to fluid-saturated porous media, and examples have been included to show the easy use and versatility of this element technology.

ACKNOWLEDGEMENTS

This research is supported by the Dutch Technology Foundation STW, which is the applied science division of NWO, and the Technology Programme of the Ministry of Economic Affairs under Project Nr. 10112.

REFERENCES

1. Rots JG. Smeared and discrete representations of localized fracture, International Journal of Fracture 1991; **51**: 45–59.
2. Schellekens JCJ, de Borst R. On the numerical integration of interface elements, International Journal for Numerical Methods in Engineering 1993; **36**: 43–66.

3. de Borst R, Crisfield MA, Remmers JJC, Verhoosel CV. Non-linear finite element analysis of solids and structures, 2nd Ed John Wiley & Sons, Chichester, 2012.
4. Segura, JM and Carol I. Coupled HM analysis using zero-thickness interface elements with double nodes. Part I: Theoretical model. International Journal for Numerical and Analytical Methods in Geomechanics 2008, **32**: 2083–2101.
5. Allix O, Ladevèze P. Interlaminar interface modelling for the prediction of delamination, Composite Structures 1992; **22**: 235–242.
6. Schellekens JCJ, de Borst R. A nonlinear finite-element approach for the analysis of mode 1 free edge delamination in composites, International Journal of Solids and Structures year 1993; **30**: 1239–1253.
7. Schellekens JCJ, de Borst R. Free edge delamination in carbon-epoxy laminates: a novel numerical/experimental approach, Composite Structures 1994; **28**: 357–373.
8. Xu XP, Needleman A. Numerical simulations of fast crack growth in brittle solids, Journal of the Mechanics and Physics of Solids 1994; **42**: 1397–1434.
9. Ingraffea AR, Saouma V. Numerical modelling of discrete crack propagation in reinforced and plain concrete. In: *Fracture Mechanics of Concrete*, pp. 171–225. Martinus Nijhoff Publishers, Dordrecht, 1985.
10. Camacho GT, Ortiz M (1996) Computational modelling of impact damage in brittle materials, International Journal of Solids and Structures **33**: 2899–2938.
11. Boone TJ, Ingraffea AR. A numerical procedure for simulation of hydraulic-driven fracture propagation in poroelastic media, International Journal for Numerical and Analytical Methods in Geomechanics 1990; **14**: 27–47.
12. Secchi S, Simoni L, Schrefler BA. Mesh adaptation and transfer schemes for discrete fracture propagation in porous materials. International Journal for Numerical and Analytical Methods in Geomechanics 2007; **31**: 331–345.
13. Belytschko T, Black T (1999) Elastic crack growth in finite elements with minimal remeshing, International Journal for Numerical Methods in Engineering **45**: 601-620.
14. Belytschko T, Moës N, Usui S, Parimi C (2001) Arbitrary discontinuities in finite elements, International Journal for Numerical Methods in Engineering **50**: 993-1013.
15. Wells GN, Sluys LJ (2001) A new method for modelling cohesive cracks using finite elements. International Journal for Numerical Methods in Engineering **50**: 2667–2682.
16. Wells GN, de Borst R, Sluys LJ (2002) A consistent geometrically non-linear approach for delamination, International Journal for Numerical Methods in Engineering **54**: 1333–1355.
17. Moës N, Belytschko T (2002) Extended finite element method for cohesive cracks. Engineering Fracture Mechanics **69**: 813–833.
18. Remmers JJC, de Borst R, Needleman A (2003) A cohesive segments method for the simulation of crack growth, Computational Mechanics **31**: 69–77.
19. de Borst R, Réthoré J , Abellan MA. A numerical approach for arbitrary cracks in a fluid-saturated porous medium. Archive of Applied Mechanics 2006, **75**: 595–606.
20. Réthoré J, de Borst R, Abellan MA. A two-scale approach for fluid flow in fractured porous media, *International Journal for Numerical Methods in Engineering* 2007, **71**: 780-800.
21. Réthoré J, de Borst R, Abellan MA. A discrete model for the dynamic propagation of shear bands in fluid-saturated medium, International Journal for Numerical and Analytical Methods in Geomechanics 2007; **31**: 347–370.
22. Réthoré J, de Borst R, Abellan MA (2008) A two-scale model for fluid flow in an unsaturated porous medium with cohesive cracks, Computational Mechanics **42**: 227-238.
23. Irzal F, Remmers JJC, Huyghe JM, de Borst R. A large deformation formulation for fluid flow in a progressively fracturing porous material. *Computer Methods in Applied Mechanics* 2013; **256**: 29–37.
24. Verhoosel CV, Scott MA, de Borst R and Hughes TJR (2011) An isogeometric approach to cohesive zone modeling, International Journal for Numerical Methods in Engineering **87**, 336-360.
25. Borden MJ, Scott MA, Evans JA, Hughes TJR. Isogeometric finite element data structures based on Bézier extraction of NURBS. *International Journal for Numerical Methods in Engineering* 2011; **87**: 15–47.
26. Scott MA, Borden MJ, Verhoosel CV, Sederberg TW, Hughes TJR. Isogeometric finite element data structures based on Bézier extraction of T-splines. *International Journal for Numerical Methods in Engineering* 2011; **88**: 126–156.
27. Bathe KJ. Finite element procedures. Upper Saddle River, NJ, USA, Prentice Hall, Inc, 1996.
28. Borden MJ, Verhoosel CV,Scott MA, Hughes TJR, Landis CM. A phase-field description of dynamic brittle fracture. *Computer Methods in Applied Mechanics and Engineering* 2012; 217220:77–95
29. Verhoosel CV, Scott MA, Hughes TJR, de Borst R. An isogeometric analysis approach to gradient damage models *International Journal for Numerical Methods in Engineering* 2011; 86:115–134
30. Piegl L, Tiller W. *The NURBS Book (Monographs in Visual Communication)*. Springer: New York, Second Edition, 1997.
31. Cottrell J, Hughes TJR, Bazilevs Y. *Isogeometric Analysis: Toward Integration of CAD and FEA*. John Wiley & Sons, Chichester, 2009.
32. Cox MG. The numerical evaluation of B-splines. *IMA Journal of Applied Mathematics* 1972; **10**: 134-149.
33. de Boor C. On calculating with B-splines. *Journal of Approximation Theory* 1972; **6**: 50-62.
34. Irzal F, Remmers JJC, Verhoosel CV, de Borst R. An isogeometric analysis approach to poroelasticity. *International Journal for Numerical and Analytical Methods in Geomechanics* 2013; DOI: 10.1002/nag.2195.
35. Remmers JJC, de Borst R, Verhoosel CV, Needleman A. The cohesive band model: a cohesive surface formulation with stress triaxiality *International Journal of Fracture* 2013; **181**(2): 177–188.